PCCP

Accepted Manuscript




ROYAL SOCIETY OF CHEMISTRY

www.rsc.org/pccp

Physical Chemistry Chemical Physics
CREATED USING THE RSC LaTeX PCCP ARTICLE TEMPLATE – SEE www.rsc.org/electronicfiles FOR DETAILS


# Heat transfer in heterogeneous nanostructures can be described by a simple chain model

**Tao Sun,[a] Jianxiang Wang,[ab] and Wei Kang*[ab]**

**We present a simple chain model for ballistic-diffusive heat transfer in heterogeneous nanostructures connected by atomistic interfaces, which are under extensive investigation for nanoscale heat transfer control. Heat transfer in typical heterogeneous nanostructures, including junctions with a single interface, multi-layered SiGe/Si systems, and nanocrystal arrays, can be well reproduced by the model. Good performance of the model in all the investigated cases shows that it captures the essential feature of interfaces connecting ballistic and diffusive thermal conducting regions. This will help to design tunable thermal transport devices and to further clarify the origin of interfacial resistance.**

With the feature size of devices continuously scaling down to the nanoscale, thermal transport at the nanoscale have recently attracted significant attention,[1–3] as it displays much wealthier features than at the macroscopic scale. In nearly perfect semi-conducting and insulating crystals, phonons may transport almost ballistically at the nanoscale. However, impurities, defects, as well as amorphous structures may give rise to phonon scatterings, which gradually lead to a diffusive heat transfer captured by the Fourier's law. Indeed, intriguing investigations to ballistic[4,5] and diffusive[6] phonon transports in various nanostructures have been reported in recent years. Ballistic transport has been confirmed in the experiments of nanocrystals,[7] single-crystalline silicon,[8] superlattices,[9] nanowires,[4] and carbon nanotubes,[5] whereas diffusive phonon transports has been observed in amorphous structures, such as nanodot layers[8], and ligands.[7] The wealthy of thermal transport behavior in different structures make it possible to manufacture heterogeneous composite materials, where some components behave ballistically while others behave diffusively. Thermal transport properties can thus be adjusted at will. This idea is reinforced by recent experimental investigations into tunable heat transfer of nanostructures, with an application to maximize the thermal conductance for cooling applications or to minimize conduction, for example, in thermoelectric applications[10–12].

[a] *State Key Laboratory for Turbulence and Complex System, Department of Mechanics and Engineering Science, College of Engineering, Peking University, Beijing 100871, China;*
[b] *HEDPS, Center for Applied Physics and Technology, College of Engineering, Peking University, Beijing 100871, China; E-mail: weikang@pku.edu.cn*

In this work, we present a simple chain model to study heat transfer in heterogeneous nanostructures, focused on coupled ballistic-diffusive transport in nanostructures where ballistic and diffusive components arranged alternatively along the direction of heat flux. With appropriately chosen parameters, details of thermal transport properties, including size effect, interfacial effect, and distribution of temperature, are well described by the model and agree well with experimental measurements as well. The good agreement with experiments in all the investigated cases implies the model an efficient theoretical tool to present the core feature of interfaces connecting ballistic and diffusive thermal conducting regions, which is valuable to further illustrate the underlying mechanism of recent experimental results on interface related heat transfer phenomena.[7,8,13–16]

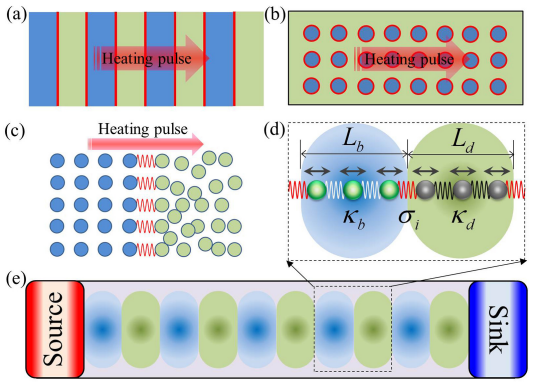


**Fig. 1** Schematics of heat transfer in nanostructures of multilayered system (a), nanocrystal array (b), a heterogeneous junction with a single interface (c); and a lattice junction (d), which is the basic unit of the chain model (e) that contains ballistic (blue) and diffusive (green) segments arranged alternatively along the direction of heat flux.

In Fig. 1(a)-(c) several heterogeneous nanostructures of particular interests to manipulate heat transfer are displayed schematically, including multi-layered systems,[7] nanocrystal arrays,[8] and heterogeneous junctions with a single interface.[13] Despite their apparent difference, these structures share a common feature, i.e., along the direction of heat flux, they can all be viewed as a chain with alternatively arranged segments, as displayed in Fig. 1(e). In each of them, phonons transport ballistically or diffusively. The basic unit, shown in Fig.1(d),

is composed of three components: a ballistic component, a diffusive component and an interface link. For heat flux along the chain, the overall thermal conductivity $\kappa$ is nominally related to thermal conductivity of each component and interfacial thermal conductance $\sigma_i$ as

$$\frac{N_bL_b+N_dL_d}{\kappa}=\frac{N_bL_b}{\kappa_b}+\frac{N_dL_d}{\kappa_d}+\frac{N_iS}{\sigma_i}, \quad (1)$$

where subscripts $b$ and $d$ denote ballistic and diffusive segment, $N$ and $L$ are number and length of each segment, and $S$ is the cross section of the structure. Unlike $\kappa_d$, $\kappa_b$ here is a rather complicated nonlinear function of size and temperature of the ballistic segment. Thermal conductivity is well defined for either ballistic or diffusive segment.[17–20] At the limit of infinitesimal temperature difference, $\kappa_{b,d}=\frac{\hbar L_{b,d}}{2\pi S}\int_0^\infty \omega\frac{\partial n(\omega)}{\partial \hat{T}}N_T\Gamma_{b,d}(\omega)d\omega$, where $\hbar$ is the Planck constant, $\omega$ is the frequency of the phonon mode, $n(\omega)$ is the density of state, $\hat{T}$ is the temperature of the component, $\Gamma(\omega)$ is the transmission coefficient, and $N_T$ is the number of transmission channels. For ballistic transport $\Gamma_b(\omega)$ is equal to 1,[17,19] whereas for diffusive transport, $\Gamma_d(\omega)$ is the ratio of the phonon's mean free path $\lambda(\omega)$ to the length of the component $L_d$.[20] But for interfacial thermal conductance, a well defined theoretical description is not available yet. Its underlying physical mechanism is still not well understood.[21,22]

At the nanoscale, thermal resistance at interfaces is comparable to those from diffusive segments and usually much larger than those from ballistic parts. An efficient approximation, even an empirical one, to the interfacial thermal conductance is then essential to interpret recent experimental discoveries. In the chain model, only the physics along the direction of heat flux is explicitly described; others are implicitly included. The system is then simplified into a one-dimensional lattice. This approach was proposed at its early stage as a simplified theoretical model for crystals,[23] and recently has been extensively employed as a tool to qualitatively understand low-dimensional heat transfer phenomena.[3,23] However, it is still not usual for the model to provide quantitative interpretation and prediction to experimental observations.

We construct the chain model in a semi-empirical way. The ballistic segment is readily described by a homogeneous harmonic lattice with nearest-neighbor interaction. The mass $\hat{m}$, lattice parameter $a$, and force constant $\hat{k}_b$ of the lattice point are associated with the density $\rho$ and elastic modulus $E$ of the segment according to $\hat{k}a^2/\hat{m}=E/\rho$, where $E$ and $\rho$ are bulk material properties that can be measured directly in an experiment. The equation of motion has a simple form of $m_i\ddot{\hat{u}}_i=\hat{f}_k^b=\hat{k}_b[(\hat{u}_{i+1}-\hat{u}_i)+(\hat{u}_{i-1}-\hat{u}_i)]$, where $\hat{u}_i$ is the displacement of the $i$-th lattice point from its equilibrium position. The diffusive segment can also be modeled as a homogeneous lattice, but with nonlinear nearest-neighbor interaction. The diffusivity is enforced by self-consistent reservoirs attaching to each of the lattice points. To keep the model simple and stable,[24] a Fermi-Pasta-Ulam $\beta$ (FPU-$\beta$) type interaction[25] is adopted for the lattice. The self-consistent reservoir takes the same form as that used in Ref. 26. Note that a nonlinear interaction here is necessary for the diffusive segment to form local equilibrium in self-consistent reservoirs. The value of $\hat{\beta}$ is chosen to be relatively small but it still provides efficient thermalization to the diffusive segment. The equation of motion for the lattice point $i$ then reads, $m_i\ddot{\hat{u}}_i=\hat{f}_k^d+\hat{f}_\beta-\hat{\gamma}_i\dot{\hat{u}}_i+\hat{P}_i(\hat{t})$. Here, $\hat{f}_k^d$ is similar to $\hat{f}_k^b$ but with a different spring constant, $\hat{\beta}$ is nonlinear cubic force constant, $\hat{f}_\beta=\hat{\beta}[(\hat{u}_{i+1}-\hat{u}_i)^3+(\hat{u}_{i-1}-\hat{u}_i)^3]$, $\hat{\gamma}_i$ is local frictional coefficient, $\hat{t}$ is time, and $\hat{P}_i(\hat{t})$ is local stochastic force, which is related to the local temperature $\hat{T}_i$ and local frictional coefficient $\hat{\gamma}_i$ through a time correlation function $\left\langle\hat{P}_i(0)\hat{P}_i(\hat{t})\right\rangle=2k_B\hat{T}_i\hat{\gamma}_i\delta(\hat{t})$, with $k_B$ being the Boltzmann constant.

Interfacial interactions between segments are modeled as harmonic springs. Preceding theoretical studies[27] have shown that higher order nonlinear interactions do not provide observable effects near room temperature, at which most experiments are carried out. Also, as demonstrated by Li *et al.*,[21] several features of interfacial thermal transport, such as its dependence on temperature difference and system size, can be described by a harmonic interaction. In practice, the value of the spring constant can be determined directly from the relation of heat flux $J$ to temperature difference $\Delta T$ cross a single interface, as displayed schematically in Fig 1(c). By fitting the chain model to the $J$-$\Delta T$ curve, the interfacial spring constant is then obtained and applied to multi-interfacial heterogeneous structures.

Putting the three parts together, a dimensionless equation of motion

$$\ddot{u}_{b,l} = f_{k,l}^b, \quad (2)$$

$$\ddot{u}_{d,l} = f_{k,l}^d+f_{\beta,l}-\gamma\dot{u}_{d,l}+P_l(t), \quad (3)$$

$$\ddot{u}_{i,l} = k_i(u_{l+1}-u_l)+k_b(u_{l-1}-u_l), \quad (4)$$

can by derived by introducing a characteristic mass $m_0$, a characteristic frequency $\omega_0$ and a length scale $a_0$, where physical quantities without hats are dimensionless, and index $l$ indicates the position of segments along the chain. The dimensionless quantities here thus represents relative magnitudes of corresponding physical quantities with respect to the reference material. To recover the real magnitude of these quantities and parameters, the units formed by the combination the three characteristic scales of the reference material should be multiplied. Explicitly, the unit of $k$ is $m_0\cdot\omega_0^2$, the unit of $u$ is $a_0$, the unit of $t$ is $\omega_0^{-1}$, the unit of $\beta$ is $m_0\cdot a_0^{-2}\cdot\omega_0^2$, the unit of $\gamma$ is $m_0\cdot\omega_0$. When experimental data are available, corresponding dimensionless parameters in the model are derived directly from the data, otherwise reasonable values are picked up to reproduce the experimental results. For $m_0$, $\omega_0$ and

$a_0$ taking typical value of solids, i.e., $m_0 \sim 10^{-26} - 10^{-27}$kg, $\omega_0 \sim 10^{13}\text{s}^{-1}$,[3] and $a_0 \sim 2\times10^{-10}$m, the dimensionless room temperature $T$ varies between 0.001 and 0.01, dimensionless $k$ is between 0.5 and 1.0, dimensionless $k_i$ is between 0.21 and 0.89, dimensionless $\beta$ is between 2.5 and 4.0, dimensionless $\gamma$ is between 0.2 and 0.25. The small magnitude of $T$ suggests a negligible scattering in the ballistic part,[28] which justifies the omitting of high order nonlinear interactions in the model.

The chain model is numerically integrated using the velocity Verlet algorithm.[29] A small time step of $5\times10^{-3}$ is employed to guarantee energy conservation. Both ends of the chain are connected to a non-reflective stochastic reservoir[27] at a temperature $T(1\pm\Delta)$, where $\Delta$ is the dimensionless temperature difference. Local thermal conductivity at the $i$-th component is defined as $\kappa = J_i L/(2ST\Delta)$, and local temperature is calculated as $T_i = \langle m_i \dot{u}_i^2 \rangle$. Both are evaluated by a combination of time average and ensemble average[25] to speed up the convergence. Even so, over $10^8$ integration steps have to be used to reach a steady state.

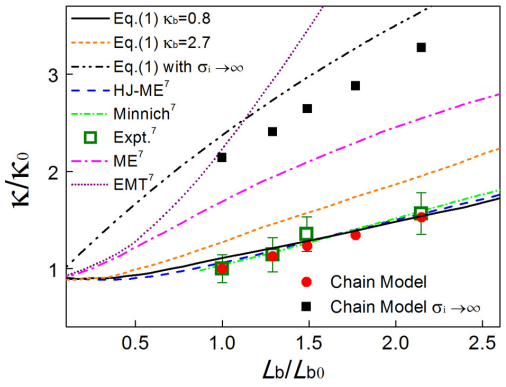


**Fig. 2** $\kappa$ as a function of $L_b$ calculated with $k_b = 1.0$, $k_d = 0.8$, $\beta_d = 4$, $\Delta = 0.2$, and $T = 0.0852$.[7] $\kappa_0$ and $L_{b0}$ are values of the first data point (i.e., $L_b/L_{b0} = 1$).

We now apply the chain model to typical heterogeneous nanostructures, in which tunable heat transfer were experimentally demonstrated. For nanocrystal arrays embedded in a continuous matrix,[7] as schematically displayed in Fig. 1(b), nanocrystal arrays are modeled as ballistic segments, whereas the continuous matrix is modeled as diffusive segments. Dimensionless parameters $k_b \sim 1$, $k_d \sim 0.8$, $T = 0.0852$, and $\Delta = 0.2$ are derived from molecular dynamics (MD) simulations which reproduce the MD results for PbS nanocrystals in Ref. 7. $k_i \sim 0.3$ is obtained from the flux-temperature relation of the single-interface experiment, and $\beta_d = 4$ is used in the model. $\kappa$'s calculated using the model are displayed as solid dots in Fig. 2, which agree well with experimental measurements,[7] shown as hollow squares with error bars.

To confirm ballistic transport in the nanocrystal, $\kappa$'s calculated using Eq. (1) with experimental data[7,30] of $\kappa_b = 2.7$ $\text{Wm}^{-1}\text{-K}^{-1}$, $\kappa_d = 0.13$ $\text{Wm}^{-1}\text{-K}^{-1}$ and $\sigma_i = 120$ $\text{MWm}^{-2}\text{K}^{-1}$ are also displayed in the same figure as short dash lines, where diffusive thermal transport is assumed for all segments. Compared with the experimental measurements, this calculation overestimates the $\kappa$'s by about 30%. To agree with the experimental data, a much smaller effective $\kappa_b = 0.8$ $\text{Wm}^{-1}\text{-K}^{-1}$ has to be used in the calculation.

The model also shows there is a finite $\sigma_i$ at the interface. Theories without $R_i$, e.g., the effective medium theory (EMT), the Maxwell Euken (ME) theory, and Eq.(1) with $\sigma_i \to \infty$ all severely overestimate $\kappa$, while those with finite $R_i$, including the modified ME model (HJ-ME) and the Minnich model, have a better agreement with the experimental results. In our model, a large $\sigma_i$ can be approximated using $k_i = 2k_b k_d/(k_b + k_d)$,[31] which also severely overestimate the $\kappa$.

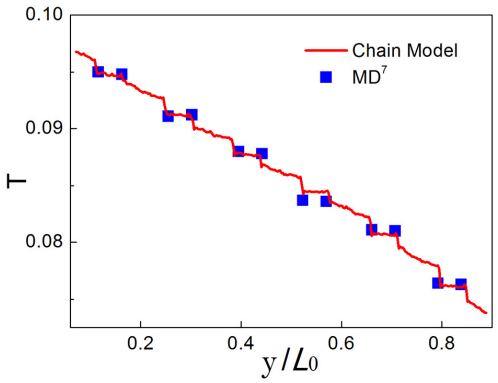


**Fig. 3** $T$ of a multi-interfacial structure along the direction of $J$, calculated with the same parameters as those in Fig. 2. $y/L_0$ is the relative position, and $L_0$ the length of the structure. Also displayed are MD results taken from Ref. 7 for comparison.

In addition to the $\kappa$, the model also provides detailed information of thermal transport in the nanostructure. Fig. 3 shows the predicted temperature distribution along the direction of heat flux, which agrees well with the MD results in Ref. 7. From the distribution, ballistic and diffusive transport can be clearly distinguished. In ballistic segments (nanocrystals), the temperature is nearly a constant due to vanishing phonon scattering,[25] whereas a significant temperature gradient is observed in the diffusive segment (continuous matrix) as the result of strong phonon scattering.

SiGe/Si multi-layered system[8] (Fig. 1(a)) is another typical heterogeneous nanostructure for heat control. In our model, the SiGe nanodots are modeled as diffusive segments separated by ballistic components made of Si spacer layers. Two system size $N_d = 5$ and $N_d = 11$ are considered according to the experiment.[8] Analogous to the previous example, parameters $k_b = 1.0$, $k_d = 0.5$, $\beta_d = 2.5$, $\Delta = 0.2$, $T = 0.0075$,[32] and $k_i = 0.31$ are used in the model. $\kappa$'s calculated with the

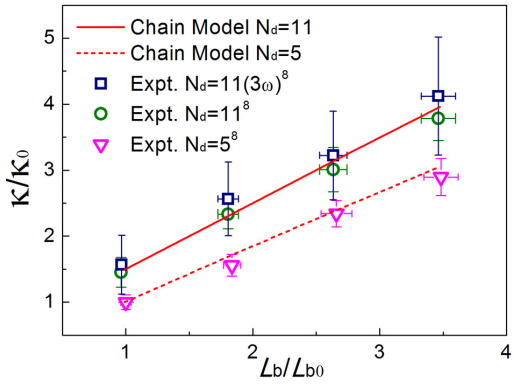


**Fig. 4** κ as a function of $L_b$ calculated with $k_b = 1.0$, $k_d = 0.5$, $\beta_d = 2.5$, $l_d = 10$, $\Delta = 0.2$, and $T = 0.0075$.[32] $\kappa_0$ and $L_{b0}$ are first data point of $N_d = 5$.

model are plotted in Fig.4 as curves, which are in good agreement with experimental measurements for the two system size $N_d = 5$ and $N_d = 11$,[8] displayed as dots in the figure. Our results clearly show that κ explicitly depends on $N_d$, which is a new feature that is not offered by the diffuse mismatch model or atomic Green's function model employed in Ref. 8.

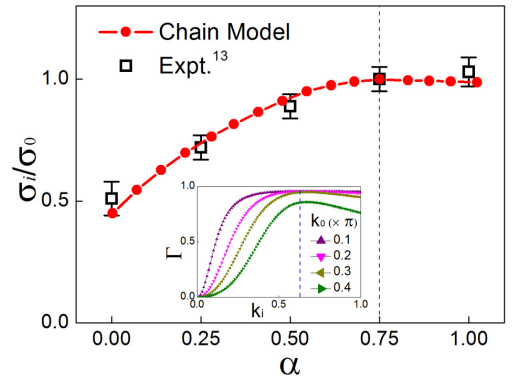


**Fig. 5** $\sigma_i$ as a function of α, the fraction of thiol end groups, calculated with $k_b = 1.0$, $N_b = 10$, $k_d = 0.5$, $\beta_d = 2.5$, $N_d = 100$, $T = 0.01$ and $\Delta = 0.2$. Inset: Γ as a function of $k_i$ for selected wave vectors $(k_0)$. The vertical dash line denotes the position corresponding to $k_i = k_i^{max}$.

A single interface (Fig.1(c)) connecting a ballistic segment and a diffusive segment is the basic unit to investigate coupled ballistic-diffusive transport and has recently been extensively studied in experiments.[13,33] Experimental measurements have revealed that interfacial thermal conductance strongly depends on the bonding strength, which is difficult to account for by either the acoustic mismatch[34] or diffuse mismatch theories.[35] For the molecular junctions studied in Ref. 13, the gold film is simplified as a diffusive segment and the self-assembled monolayer is modeled as a ballistic segment. Terminal functional groups of various bonding strength between the gold film and monolayer is modeled as the interfacial connection of a certain $k_i$. For an interface composed of methyl/thiol end-groups, $k_i$ is proportional to the fraction α of thiol end-groups, which form strong covalent-like bonds between the gold film and monolayer.[13] With the parameters $k_b = 1.0$, $N_b = 10$, $k_d = 0.5$, $\beta_d = 2.5$, $N_d = 100$, $T = 0.01$ and $\Delta = 0.2$, a thermal conductance $\sigma_i$, displayed in Fig. 5 as solid dots, can thus be calculated as a function of bonding strength. The calculated $\sigma_i$ increases first until it reaches its maximum value corresponding to $k_i = k_i^{max} = 2k_bk_d/(k_b + k_d)$, the interfacial interaction value allowed for maximum heat flux going through the interface.[31] After that, $\sigma_i$ decreases very slowly. Experimental data[13] in Fig. 5 suggest that $k_i^{max}$ takes place near $\alpha = 0.75$. With this data point, the relation between $k_i$ and α is determined as $k_i = 0.61\alpha + 0.21$. When plotted as a function of α, the calculated $\sigma_i$ shows a good agreement with the experimental data.[13] Note that the $\sigma_i$ from the quartz-monolayer interface[13], which is a constant, is deducted from the experimental data to compare with the model.

To further understand the mechanism of heat transfer, we perform phonon wave packet dynamic simulations[36] for the single interface. The transmission coefficient (Γ) is calculated as the ratio of transmitted energy ($E_{tr}$) to the incident ($E$) energy of the wave-packets, i.e., $\Gamma = E_{tr}/E$. The inset of Fig. 5 shows that Γ increases with $k_i$ to a maximum value at $k_i^{max}$ and then decreases slowly. This result provides a further justification to the result of $\sigma_i$ displayed in Fig. 5.

In summary, we present a simple chain model for ballistic-diffusive heat transfer in heterogeneous nanostructures connected by atomistic interfaces. In addition to its capability to interpret recent experiments, the model is also demonstrated as a simple but nontrivial tool to describe interfaces connecting ballistic and diffusive thermal conducting regions, including all major features for the interfaces. This would help to design devices for heat transfer control and to clarify the origin of interfacial thermal resistance.

## Acknowledgements

This work is supported by the National Natural Science Foundation of China (Grant no. 10932001), and Major State Basic Research Development Program of China (Grant no. 2011CB013101).

## References

1 T. F. Luo and G. Chen, *Phys. Chem. Chem. Phys.*, 2013, **15**, 3389.
2 D. G. Cahill, P. V. Braun, G. Chen, D. R. Clarke, S. H. Fan, K. E. Goodson, P. Keblinski, W. P. King, G. D. Mahan, A. Majumdar, H. J. Maris, S. R. Phillpot, E. Pop and L. Shi, *Appl. Phys. Rev.*, 2014, **1**, 011305.
3 N. B. Li, J. Ren, L. Wang, G. Zhang, P. Hanggi and B. W. Li, *Rev. Mod. Phys.*, 2012, **84**, 1045.

4 T. K. Hsiao, H. K. Chang, S. C. Liou, M. W. Chu, S. C. Lee and C. W. Chang, *Nat. Nanotech.*, 2013, **8**, 534.

5 N. Mingo and D. A. Broido, *Phys. Rev. Lett.*, 2005, **95**, 096105.

6 A. Lervik, F. Bresme, S. Kjelstrup, D. Bedeaux and J. M. Rubi, *Phys. Chem. Chem. Phys.*, 2010, **12**, 1610.

7 W. L. Ong, S. M. Rupich, D. V. Talapin, J. H. McGaughey and J. A. Malen, *Nature Mater.*, 2013, **12**, 410.

8 G. Pernot, M. Stoffel, I. Savic, F. Pezzoli, P. Chen, G. Savelli, A. Jacquot, J. Schumann, U. Denker, I. Monch, Ch. Deneke, O. G. Schmidt, J. M. Rampnoux, S. Wang, M. Plissonnier, A. Rastelli, S. Dilhaire and N. Mingo, *Nature Mater.*, 2010, **9**, 491.

9 M. N. Luckyanova, J. Gang, K. Esfarjani, A. Jandl, M. T. Bulsara, A. J. Schmidt, A. J. Minnich, S. Chen, M. S. Dresselhaus, Z. F. Ren, E. A. Fitzgerald and G. Chen, *Science*, 2012, **338**, 936.

10 M. Zebarjadi, K. Esfarjani, M. S. Dresselhaus, Z. F. Ren and G. Chen, *Energy Environ. Sci.*, 2012, **5**, 5147.

11 Z. T. Tian, S. Lee and G. Chen, *J. Heat Transfer*, 2013, **135**, 061605.

12 G. J. Snyder and E. S. Toberer, *Nature Mater.*, 2008, **7**, 105.

13 M. D. Losego, M. E. Grady, N. R. Sottos, D. G. Cahill and P. V. Braun, *Nature Mater.*, 2012, **11**, 502.

14 P. J. O'Brien, S. Shenogin, J. X. Liu, P. K. Chow, D. Laurencin, P. H. Mutin, M. Yamaguchi, P. Keblinski and G. Ramanath, *Nature Mater.*, 2013, **12**, 118.

15 B. Gotsmann and M. A. Lantz, *Nature Mater.*, 2013, **12**, 59.

16 M. E. Siemens, Q. Li, R. Yang, K. A. Nelson, E. H. Anderson, M. M. Murnane and H. C. Kapteyn, *Nature Mater.*, 2010, **9**, 26.

17 J. S. Wang, J. Wang and J. T. Lu, *Eur. Phys. J. B*, 2008, **62**, 381.

18 G. F. Xie, Y. Guo, B. H. Li, L. W. Yang, K. W. Zhang, M H. Tang and G. Zhang, *Phys. Chem. Chem. Phys.*, 2013, **15**, 14647.

19 C. Jeong, S. Datta and M. Lundstrom, *J. Appl. Phys.*, 2012, **111**, 093708.

20 N. Mingo, *Phys. Rev. B*, 2003, **68**, 113308.

21 B. Li, J. Lan and L. Wang, *Phys. Rev. Lett.*, 2005, **95**, 104302.

22 J. W. Zhang, C. Jiang, D. Z. Jiang and H. X. Peng, *Phys. Chem. Chem. Phys.*, 2014, **16**, 4378.

23 R. Livi and S. Lepri, *Nature* (London), 2003, **421**, 327.

24 N. W. Ashcroft and N. D. Mermin, Solid State Physics, 1976, Harcourt, Orlando.

25 S. Lepri, R. Livi and A. Politi, *Phys. Rep.*, 2003, **377**, 1.

26 A. Dhar, *Adv. Phys.*, 2008, **57**, 457.

27 T. Sun, J. Wang and W. Kang, *Europhys. Lett.*, 2014, **105**, 16004.

28 B. Hu, B. Li and H. Zhao, *Phys. Rev. E*, 2000, **61**, 3828.

29 M. P. Allen and D. J. Tildesley, Computer Simulations of Liquids, 1987, Clarendon, Oxford.

30 Y. L. Pei and Y. Liu, *J. Alloys Compd.*, 2012, **514**, 40.

31 L. F. Zhang, P. Keblinski, J. S. Wang and B. W. Li, *Phys. Rev. B*, 2011, **83**, 064303.

32 E. R. Cowley, *Phys. Rev. Lett.*, 1988, **60**, 2379.

33 P. E. Hopkins, L. M. Phinney, J. R. Serrano and T. E. Beechem, *Phys. Rev. B*, 2010, **82**, 085307.

34 W. A. Little, *Can. J. Phys.*, 1959, **37**, 334.

35 E. T. Swartz and R. O. Pohl, *Rev. Mod. Phys.*, 1989, **61**, 605.

36 P. K. Schelling, S. R. Phillpot and P. Keblinski, *Appl. Phys. Lett.*, 2002, **80**, 2484.

# A table of contents entry

Physical Chemistry Chemical Physics

CP-COM-04-2014-001843

23-June-2014

1. The novelty of the work:

**Heat transfer in heterogeneous nanostructures is captured by a simple 1D chain model, agreeing well with experiments.**

2. Colour graphic: maximum size 8cm x 4cm